Strengthening of lateral activation in adult rat visual cortex after retinal lesions captured with voltage-sensitive dye imaging in vivo

Ganna Palagina[a,b,c], Ulf T. Eysel[b,c], and Dirk Jancke[a,c,d,1]

[a]Cognitive Neurobiology, [b]Department of Neurophysiology, [c]International Graduate School of Neuroscience, and [d]Bernstein Group for Computational Neuroscience, Ruhr University Bochum, D-44780 Bochum, Germany

Edited by Jon H. Kaas, Vanderbilt University, Nashville, TN, and approved March 17, 2009 (received for review January 6, 2009)

Sensory deprivation caused by peripheral injury can trigger functional cortical reorganization across the initially silenced cortical area. It is proposed that intracortical connectivity enables recovery of function within such a lesion projection zone (LPZ), thus substituting lost subcortical input. Here, we investigated retinal lesion-induced changes in the function of lateral connections in the primary visual cortex of the adult rat. Using voltage-sensitive dye recordings, we visualized in millisecond-time resolution spreading synaptic activity across the LPZ. Shortly after lesion, the majority of neurons within the LPZ were subthresholdly activated by delayed propagation of activity that originated from unaffected cortical regions. With longer recovery time, latencies within the LPZ gradually decreased, and activation reached suprathreshold levels. Targeted electrode recordings confirmed that receptive fields of intra-LPZ neurons were displaced to the retinal lesion border while displaying normal orientation and direction selectivity. These results corroborate the view that cortical horizontal connections have a central role in functional reorganization, as revealed here by progressive facilitation of synaptic activity and the traveling wave of excitation that propagates horizontally into the deprived cortical region.

horizontal connections | plasticity | striate cortex

The adult cerebral cortex is capable of plastic reorganization that can partially recover lost function (1–7). In primary visual cortex, a focal retinal lesion cuts off retinal input, leading to a cortical region in which no visually evoked spikes can be detected. However, after a given period of recovery, initially redundant neurons regain responsiveness, with receptive fields shifted toward positions represented by neurons at the border of the lesion projection zone (LPZ) (2–4, 8–11), even within hours after lesion (12, 13).

A common hypothesis is that long-range horizontal cortical connections, originating in extragranular cortical layers, substitute for deprived thalamic input, thereby enabling LPZ neurons to share function with their unaffected neighbor cortical neurons (6). Indeed, 2-photon imaging in mouse visual cortex showed a 3-fold increase in loss and gain of dendritic spines in layer 2/3, arguing for remodeling of horizontal connectivity (14). Earlier, it also had been shown that axonal sprouting may be involved in long-term cortical reorganization (15). Moreover, intrinsic optical imaging revealed recovery of an orientation map to a layout similar to the one before lesion (8). Such preservation of orientation preference despite the shift of receptive fields is indicative of massive restructuring of the existing intracortical network, involving large populations of neurons within and outside the lesion-affected cortex.

However, single-cell recordings are limited in spatial sampling, and therefore they do not provide a coherent population picture of activation across the LPZ. Moreover, spiking activity reports the binary outcome of far-reaching integrative processes but not their underlying analogue synaptic events. Thus, gradual changes in subthreshold synaptic activity over the time span of recovery processes cannot be revealed. Intrinsic optical imaging and fMRI, on the other hand, enable sampling of large cell populations but are limited in temporal resolution. Furthermore, the recorded hemodynamic signals are only indirectly coupled to electrical activity and fail to disambiguate subthreshold synaptic events from mass suprathreshold activation.

For these reasons, we made use of a high-resolution imaging technique that employs voltage-sensitive dye, emphasizing postsynaptic dendritic potentials (16), to explore the dynamic changes in functional properties of lateral connections over the time course of cortical reorganization at the neuronal population level.

Results

Visual input to the medial monocular part of rat primary visual cortex was removed by laser coagulation of a small, ≈1-mm-diameter, patch of the upper retina just dorsal to the optic disc. The lesion resulted in destruction of all retinal layers and fibers of passage, leading to formation of a scotoma of 15–20° temporonasal width and extending from below the optic disc to the far periphery of the monocular lower visual field (Fig. 1 *A*, *B*, and *D*). Measurements were performed in 3 groups of animals: 2 groups of rats were lesioned at postnatal day 65 (P65) and recorded either at P69–P72 (acute lesion) or after a longer period of recovery, at P92–P105. Unlesioned rats of matching ages were used in control experiments to delineate normal retinotopy.

To determine the initial position and extension of the LPZ functionally, retinotopic mapping was performed by using voltage-sensitive dye imaging (VSDI; Fig. 1*B*). Apart from the affected lower central position (red), each stimulated locus in the visual field was represented by a local spot of activity (Fig. 1*C* depicts the complete retinotopic map for an unlesioned control). Fig. 1*D* summarizes the cortical retinotopic organization after lesion. Because of the cortical point-spread function, activated regions were partially overlapping, in sum representing ≈60 × 60° of the visual field, excluding the lesioned region that was cortically neglected (dotted line in Fig. 1*D* marks border of the LPZ, shaded in gray).

Next, we measured responses to full-field stimuli that entirely covered the sampled visual field, including the scotoma. Fig. 2*A* depicts the response dynamics for 2 different cases at 6 and 28 days after lesion (Fig. 2*A Upper* and *Lower*, respectively). At the onset of response, both animals revealed an instantly activated cortical region (greenish areas in 60-ms frames), reflecting early vertical input to the lateral part of the cortex unaffected by the lesion. Fig. 2*B* shows the corresponding latency maps in which

Author contributions: G.P., U.T.E., and D.J. designed research; G.P., U.T.E., and D.J. performed research; G.P. and D.J. analyzed data; and D.J. wrote the paper.

The authors declare no conflict of interest.

This article is a PNAS Direct Submission.

[1]To whom correspondence should be addressed. E-mail: jancke@neurobiologie.rub.de.

This article contains supporting information online at www.pnas.org/cgi/content/full/0900068106/DCSupplemental.

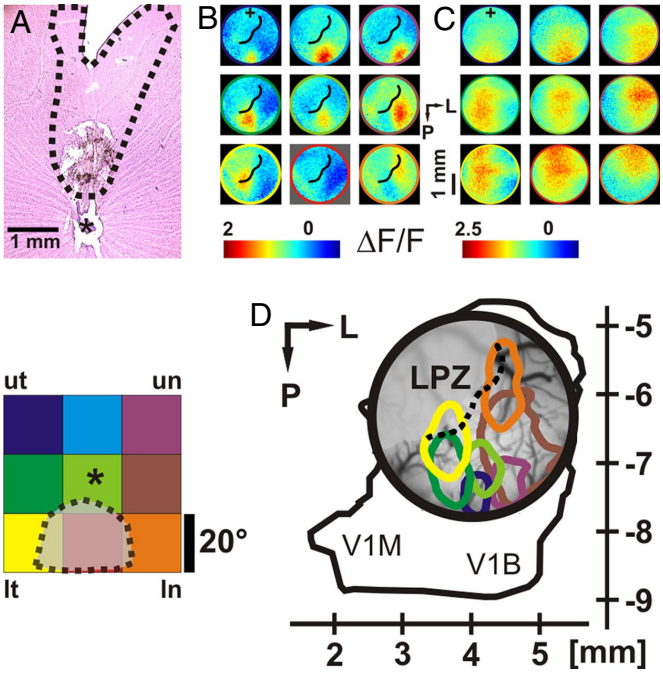

Fig. 1. Monocular retinal lesion produces a circumscribed loss of input to primary visual cortex. (*A*) Photograph from a Nissl-stained retinal wholemount from the left eye. Note the optic disc (asterisk), the adjacent direct laser lesion in the dorsal retina, and the dorsally extending region of retrograde ganglion cell degeneration that add up to the complete area of visual loss in the retina (broken line). For further details, see *Methods*. (*B*) Cortical retinotopy 6 days after lesion. VSDI signals were averaged over the first 50 ms of responses. Colorbar indicates levels of activity (ΔF/F, see *Methods*). Black line marks the border of the LPZ. (*C*) Unlesioned control. Note that the lower central stimulus (red) evoked early activity in those regions that were unresponsive in *B*. (*D*) (*Left*) Retinotopic stimuli (20°) were arranged within a 3 × 3 grid. Color codes stimulus identity; stimulus position: ut/lt, upper/lower temporal; n, nasal. Gray patch sketches lesion-affected location in visual field coordinates. Asterisk marks projection of the papilla. (*Right*) Retinotopic cortical map of significantly activated regions as depicted in *B*. Because of the retinal lesion, cortical regions beyond the LPZ border (dotted line) do not receive direct input. Position of the recording chamber is indicated by coordinates: P, posterior relative to Bregma; L, lateral from midline; V1M, monocular V1; V1B, binocular V1. Small cross in *B* and *C* marks 5 mm P, 4 mm L.

earliest responses can be seen along the lateral posterior–anterior axis (green colors). Starting from this region, both examples showed a gradual increase in latencies toward medial (red-gray), indicating delayed propagation of activity into the LPZ. The gradual spread of activity into the LPZ is depicted in 20-ms time frames in Fig. 2*A*. Although activity continued to rise at initial input regions, low-level activity crossed the LPZ border (black line) at which horizontal input starts dominating thalamic contributions (see Fig. S1, in which horizontal spread was uncovered by using an artificial scotoma). Fig. 2*C* shows traces of activity across pixels representing unaffected regions (green), LPZ border (red), and the LPZ (gray). The gradual shift of the curves shows the systematic increase in latencies across the LPZ. Importantly, the slope of the latency gradient across the LPZ was significantly steeper in the acutely lesioned animal compared with 28 days after lesion (Fig. 2 *B* and *C Lower*: curves appear compressed, demonstrating a rapid subsequent activation). In addition, amplitudes reached within the LPZ relative to unaffected regions were lower after brief recovery (Fig. 2*D*).

For statistical analysis, we divided all treated animals into 2 groups: those measured shortly after lesion (I: 4–7 days, $n = 6$) and those that had recovered for a longer time (II: 28–44 days, $n = 6$). For both groups, unaffected cortical regions had similar latencies (I, 98.8 ms; II, 97.2 ms after stimulus onset; Fig. 3*A*). For animals measured several days after lesion, latencies within the center of the LPZ (860 μm from the border) were ≈28 ms delayed (126 ± 5 ms) compared with unaffected regions. In contrast, after longer recovery, latencies within the LPZ were delayed by only ≈12 ms (108 ± 2 ms) and were almost similar across the entire LPZ (Fig. 3*A*, compare dark and light gray bars). This effect was paralleled by a significant increase in amplitudes within the LPZ, reaching ≈80% of values obtained across intact regions (Fig. 3*B*). Both progressive shortening of latencies and increased maximal amplitudes point to increased efficacy in synaptic transmission within the LPZ after prolonged recovery. The VSDI signal originates mainly from superficial layers (>80%) due to focal depth, penetration depth of the dye, and light scattering (16). Hence, potential remodeling in deeper cortical layers or changes in thalamocortical afferents cannot be observed directly. Neurons in layers 5/6 contribute, however, to the optical signal because they possess dendritic arbors in layers 2/3.

Even though the voltage-sensitive dye signal reports changes in synaptic potentials across several millimeters of cortex with high temporal accuracy, spike events are not detected by the signal (17–19). Thus, to test whether higher fluorescence levels correspond to suprathreshold activity, we performed additional electrophysiological recordings. Starting from the border of the LPZ, spiking activity could be evoked as far as 0.8–1 mm within the LPZ (Fig. 4 *A* and *B*, red/orange/black). As expected, the corresponding receptive fields (Fig. 4*C*, bold-outlined rectangles) were shifted away from their normal retinotopic positions and clustered at the border of the lesion-affected visual space (Fig. 4*C*, gray shaded area). Moreover, we found that many neurons responded to stimulus orientation and direction (polar plots in Fig. 4*B*). Although orientation tuning varied across a broad range, selectivity of neurons within the LPZ was not significantly different from units located in unaffected cortex (Fig. S3 summarizes all experiments), as observed similarly in the literature (20). Hence, in animals that were allowed to recover for several weeks, electrophysiology proved that the increased amplitudes of the dye signals within the LPZ were indeed reflecting suprathreshold activity. In contrast, no spikes could be evoked within the LPZ of animals up to 1 week of recovery (Fig. S4). Thus, the observed lateral spread of activity from unaffected cortical regions into the LPZ remained largely subthreshold within the group measured 4–7 days after lesion.

Discussion

We explored, by using VSDI, plasticity of the adult visual cortical circuitry triggered by monocular retinal lesions in the rat. As a consequence of removal of dominant afferent input, intracortical lateral spread was unmasked, originating from unaffected cortical regions. Within a short period of recovery, remote inputs from neurons ≈1 mm outside the LPZ remained subthreshold. After several weeks of recovery, however, stimulus-related suprathreshold activity within the LPZ was obtained. Our observations suggest that gradual reinforcement of horizontal inputs may compensate for lesion-induced loss of function in vertical projections.

Challenging Findings. By using metabolic markers, such as cytochrome oxidase (21) or hemodynamic signals (22), previous investigations in monkey primary visual cortex (V1) could not confirm cortical reorganization after binocular retinal lesions, as opposed to refs. 2, 3, 8, and 14. Two explanations may exist for our positive results and the discrepancies in comparison with results with metabolic markers.

First, interspecies differences in cortical magnification factors could account for various extents of LPZ filling-in. In the cited studies (21, 22), retinal lesions affected visual cortical representations covering 4–12° of visual space. Thus, full recovery of the

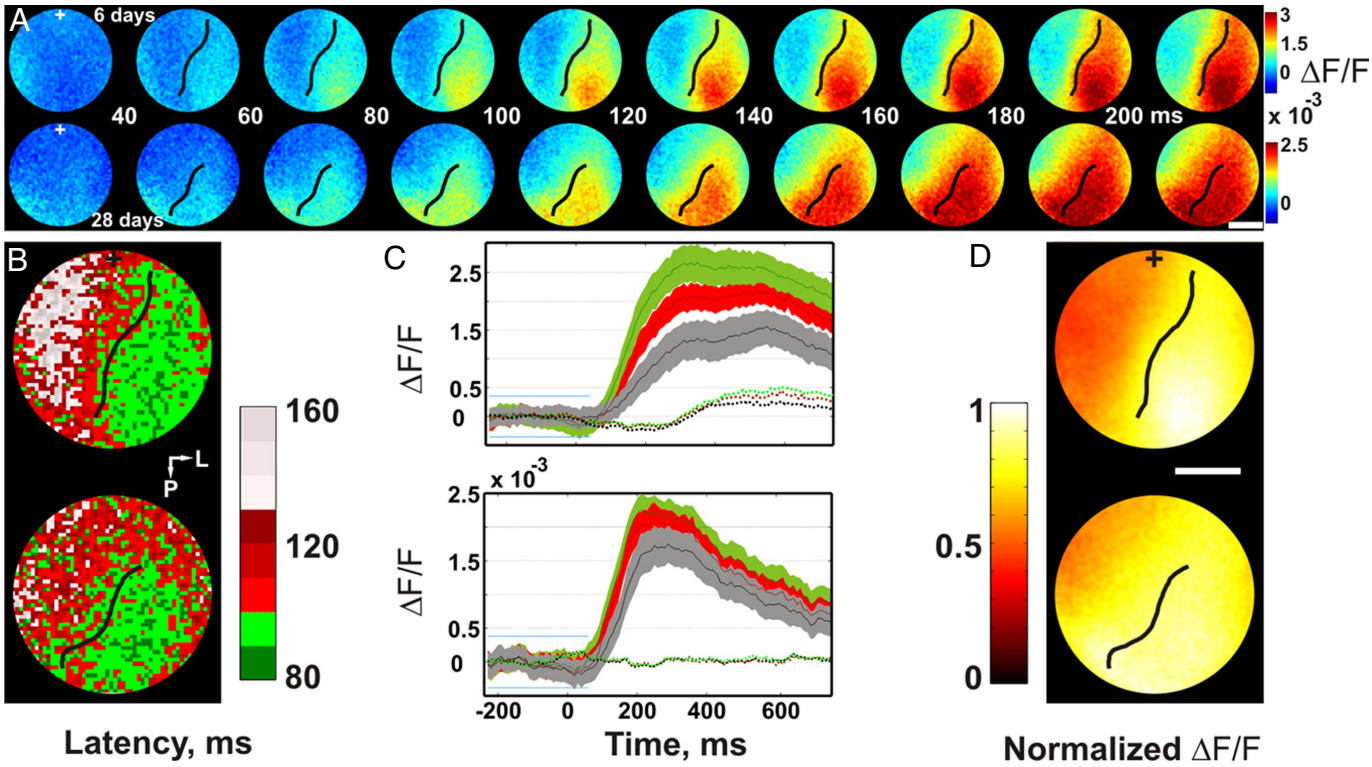

Fig. 2. Lateral spread of cortical activity across the LPZ. (*A*) Single snapshots of evoked VSDI signals. Colorbars show activity levels, same conventions as in Fig. 1 *B* and *C*. (*Upper*) Six days after lesion. (*Lower*) Twenty-eight days after lesion. Black line in images marks LPZ border. High-amplitude activity propagates beyond the border of the LPZ after 28 days of recovery (see Movie S1 for a 10-ms time resolution). (*B*) Latencies as a function of cortical site. Each pixel's latency was evaluated by determining the time at which activity crossed prestimulus levels (see *Methods*). Note that after 28 days of recovery (*Lower*), latencies within the LPZ were decreased compared with 6 days after lesion (*Upper*). (*C*) Time courses averaged across pixels outside (green), on the border (red), and inside (gray) the LPZ. Solid lines depict mean, and colored contours show 1 SD. Blue lines mark ±2 SD from baseline, and dotted lines depict activity without stimulation. The later phase of the responses often varied unsystematically across animals and was independent of postlesion times. (*D*) Relative activity levels within LPZ and over unaffected cortex. Values were normalized to maximum value reached across all pixels (see colorbar). (*Upper*) Six days after lesion, most of the pixels within the LPZ reached values of only ≈60% of unaffected regions. This value increased to ≈80% with longer recovery (*Lower*). (Scale bars: 1 mm.)

LPZ in monkey would have to involve cortical regions of many square millimeters, demanding far-reaching remodeling of connectivity. Here, as in ref. 14, rodents were used in which each millimeter of visual cortex contains neurons with dense overlap of dendritic and axonal trees, covering a much larger visual space compared with primate V1. Therefore, strengthening of horizontal connectivity within a millimeter of rodent V1 leads to functional recovery of up to 20° in visual field coordinates. In addition, spine turnover rate, indicating potential plasticity, was found to be ≈8 times higher in mouse compared with macaque visual cortex (23).

Second, metabolic markers do not report cortical activity directly but generate signals that are slow compared with the underlying neuronal events. Therefore, the position of the actual border of the LPZ might be underestimated based on fMRI signals that dominantly reflect integration of input rather than spiking output (24). The time-averaged hemodynamic signal may include both components, summing lateral input into the LPZ as well as retinotopically evoked spikes, eventually smearing the exact position of the LPZ. In our study, the high spatiotemporal resolution of VSDI allowed separation between lateral and direct cortical input by detecting latency differences of synaptic activity (25).

Ultimately, more studies are needed that describe "filling-in" after loss of retinal input to investigate the degree and the quality of functional recovery at behavioral levels (26–28) in parallel with physiological measurements.

Reinforcement of Lateral Activation: Structural and Functional Synaptic Changes. Lesion-induced strengthening of lateral activation, as observed here, must be reflected by structural changes at the single-neuron level. By using 2-photon imaging in mouse visual cortex, a recent study demonstrated a 3-fold increase in dendritic spine turnover several days after retinal lesion (14). During a recovery period of 2 months, ≈90% of spines at apical dendrites of layer 5 neurons were replaced. The authors also showed that such remodeling of synaptic contacts inside the LPZ depended on input from neighboring cortical regions because animals with complete binocular lesions revealed only a little increase in spine dynamics. Axonal projections in rat area 17 extend up to 1.8 mm in layers 2/3, 5, and 6 (29). Thus, increased spine turnover (14, 23) and changes in dendritic field morphology (30–32) might serve as a basis for functional reorganization within the existing long-range axonal plexus. Axonal sprouting, as an additional anatomical substrate for strengthening of lateral input, was found in cat visual (15) and in mouse and monkey somatosensory (33, 34) but not in rodent visual cortex (14). Therefore, to what extent axonal growth in rodent visual cortex plays a critical role in remodeling of intracortical connectivity remains unclear.

At the synaptic level, increased glutamate concentrations (35, 36), decreased GABA concentrations, and glutamic acid decarboxylase expression (37, 38) after lesion all contribute to net hyperexcitability as revealed around the border of the LPZ in cat visual cortex. During the recovery process, this region propagates into the LPZ, paralleled by a constant shrinkage of the

NEUROSCIENCE

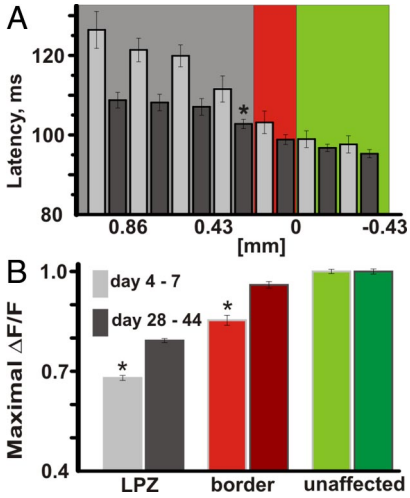

Fig. 3. Summary of VSDI experiments: effect of postlesion time on changes in synaptic cortical activity at different cortical regions (color code as in Fig. 2*C*): 4–7 days after lesion (dark gray) and 28–44 days after lesion (light gray). (*A*) Latencies at different cortical recording sites. Both groups had similar latencies across lesion-unaffected cortical regions (−0.43 to 0 mm) up to 0.2 mm from the LPZ border (red). Inside the LPZ, latencies increased differently for short recovery compared with the group with longer recovery times (*, $P <$ 0.05). Propagation speed of activity: for short recovery, 0.03–0.05 m/s; for long recovery, 0.08–0.11 m/s. (*B*) Effect of postlesion times on response amplitudes (bright colors denote 4–7 days after lesion). For each individual experiment, amplitudes of activity over unaffected cortex (green) were normalized to one. Error bars are SE.

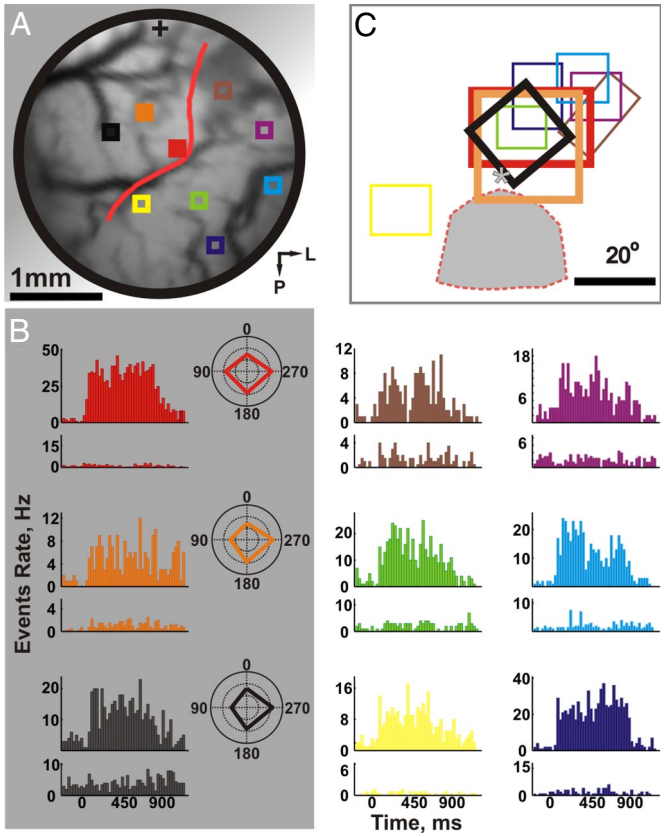

Fig. 4. Electrophysiological confirmation of functional recovery 32 days after lesion. (*A*) Vascular image and recording sites before VSDI. Red line marks LPZ border. (*B*) Poststimulus time histograms (PSTHs) of neurons recorded at locations shown in *A*; colors match recording sites. Lower graphs in each pair present spontaneous activity. Neurons within the LPZ (gray background) were responsive to drifting gratings and showed various degrees of direction tuning (see polar plots). Each histogram displays activity evoked by preferred grating orientation. (*C*) Receptive fields of neurons within the LPZ (outlined bold) appeared at the border of the lesion's projection (gray; asterisk indicates projection of papilla). Neurons outside the LPZ showed normal retinotopic arrangements of receptive fields. Receptive fields were hand mapped. See Fig. S2 for another example, 29 days after lesion.

initially nonresponsive area (9, 35). Although we could not find hyperexcitability reflected in the dye signal, possibly because of low signal to noise ratio close to baseline, our electrical recordings frequently revealed units with high spontaneous activity (Fig. S4). Hyperexcitability due to lesion-induced shifts in the excitation–inhibition balance (39) may create the basis for enhancement of synaptic transmission via horizontal fibers through long-term potentiation-like mechanisms (40). Additionally, as horizontal input leads intra-LPZ responses during the recovery process, the reversal of spike order may trigger spike time-dependent plasticity (STDP)-like alterations in synaptic transmission. Indeed, computational models implicate STDP-dependent reorganization after monocular retinal lesion in cat or after whisker trimming in rat barrel cortex (41, 42). At the population level, these plastic changes in synaptic transmission are most likely reflected by strengthened lateral activation, as observed in our study.

Methods

All surgical and experimental procedures were approved by the German Animal Care and Use Committee (AZ 50.8735.1) in accordance with the Deutsche Tierschutzgesetz and the National Institutes of Health guidelines. A total of 18 healthy adult (9–14 weeks old) Agouti Brown rats were used for the experiments.

Retinal Lesions. The left retinae of ketamine/xylazine-anesthetized adult rats were focally photocoagulated by a high-intensity laser lesion (1 mm, 1,000 mW, 200–300 ms) through a laser-adapted operating microscope. The resulting round lesions were localized in the retina dorsal to the optic disc and typically extended about 1 mm horizontally (corresponding to 15°-20° along the horizontal meridian in visual space). The lesion destroyed all retinal layers, including axonal fibers of passage, leading to retrograde degeneration of all retinal ganglion cells peripheral to the lesion, which extends the scotoma from the lesion proper toward the far periphery of the monocular lower visual field.

Animal Preparation. Experiments were performed under general anesthesia. After premedication with 0.05 mg kg^{-1} atropine sulfate, anesthesia was induced with chloral hydrate (4%, 1 mL 0.1 kg^{-1}). Xylocaine (4%) was used for additional local anesthesia. Animals were tracheotomized and artificially ventilated (0.8–1.1% isofluorane, 40% O_2, 60% N_2O, 1–1.2 Hz). End-tidal CO_2 was measured constantly and kept at 3.8–4.2%. Heart rate and body temperature (37–38°C) were monitored during the entire experiment. Craniotomy was performed over the right primary visual cortex (3–9 mm posterior to Bregma; 1–5 mm lateral). Subsequently, a metal chamber was attached to the skull. During imaging sessions, the chamber was filled with artificial CSF and sealed with a coverslip. During the experiments, animals received an i.v. infusion of electrolytes (Sterofundin; Braun), 2.5% glucose, and alcuronium chloride (Alloferin, Valeant Pharmaceuticals) to block eye movements (0.06 mg kg^{-1} h^{-1}). The eyes were regularly flushed with hyperosmotic saline. Before measurements the pupils were dilated with atropine.

Visual Stimulation. Visual stimuli were generated by VSG (Cambridge Research Systems Ltd.), controlled by a custom-written Matlab routine, and displayed on a 24-inch Sony monitor (GDM-FW900; 100 Hz). Stimuli were presented at a 30-cm distance to the contralateral eye, covering ≈60 × 60°. The position of the papilla projection was mapped onto the screen by using ophthalmoscope backprojection and was repeatedly measured to check for residual eye movements. Full-field stimuli consisted of vertical and horizontal square wave gratings (0.02 cycles per degree; 2 cycles per second). For retinotopic mea-

surements grating size was 20 × 20°, presented within a 3 × 3 grid. Mean luminance of the stimuli was 57 cd/m^2. Each stimulus (750-ms presentation time) was alternated with an interstimulus period (15 s) in which an isoluminant gray background (blank) was shown. To measure baseline activity, 2 blanks were included in each trial consisting of all stimulus conditions presented in pseudorandom order.

Electrophysiology. Before imaging, electrophysiological recordings (glass-coated tungsten, 1–2 MOhm) were performed through the intact dura. Recording depth was 300–500 μm, corresponding to units located in layer 2/3. Receptive field positions were either hand-mapped or quantified by retinotopic measurements. Histograms were calculated by averaging (20–60 stimulus repetitions).

VSDI. After the dura was carefully removed, the cortex was stained for 2 h with blue voltage-sensitive dye (RH-1838). Subsequently, unbound dye was washed out with artificial CSF. Imager 3001 (Optical Imaging Inc.) was used with a tandem lens macroscope, 85 mm/1.2 toward camera and 50 mm/1.2 toward subject. The camera was focused ≈400–500 microns below cortical surface. The cortex was illuminated with 630 ± 10 nm light, and emitted light was high-pass filtered with a cutoff at 665 nm using a dichroic filter system. Frames were collected at 100 Hz.

Data Analysis. ***Processing of raw imaging data.*** Normalization was performed for each pixel by its DC level during the prestimulus period (200 ms). Next, heartbeat and respiration-related artifacts were removed by dividing by the average of blank signals recorded in absence of stimulation. These steps were applied for each trial separately and then averaged across trials (n = 20–30).

Determination of the LPZ. First, activity of all grating conditions was averaged. Significance of stimulus-evoked responses was then estimated by using bootstrap with replacement over single trials. For each image pixel and each time frame, P values were derived by comparison to prestimulus conditions using ANOVA. The resulting P value maps were smoothened (Butterworth; filter size 270 microns), and latencies of pixels were calculated by determining the time of significant response ($P < 0.05$). The unaffected cortical region was characterized by earliest latencies and includes pixels that crossed significance threshold in 3 consecutive time frames. The border of the LPZ outlines pixels with longer latencies. For the calculation of propagation velocities, profiles parallel to the LPZ border were created (by using unfiltered P value maps). Velocity was calculated perpendicular to these strips (width 4 pixels = 215 microns). The slope of the curves from linear regression of latencies is equal to speed.

ACKNOWLEDGMENTS. We thank Herman Korbmacher for excellent handmade electrodes, Ute Neubacher for producing retinal wholemounts, and Winfried Junke for help with spike acquisition software (National Institute of Mental Health CORTEX; see www.cortex.salk.edu/). This work has been financed by the Federal Ministry of Education and Research (D.J.), Deutsche Forschungsgemeinschaft SFB 509 (to U.T.E.), and the International Graduate School of Neuroscience.

1. Kaas JH, et al. (1990) Reorganization of retinotopic cortical maps in adult mammals after lesions of the retina. *Science* 248:229–231.
2. Gilbert CD, Wiesel TN (1992) Receptive field dynamics in adult primary visual cortex. *Nature* 356:150–152.
3. Heinen SJ, Skavenski AA (1991) Recovery of visual responses in foveal V1 neurons following bilateral foveal lesions in adult monkey. *Exp Brain Res* 83:670–674.
4. Schmid LM, Rosa MG, Calford MB, Ambler JS (1996) Visuotopic reorganization in the primary visual cortex of adult cats following monocular and binocular retinal lesions. *Cereb Cortex* 6:388–405.
5. Buonomano D, Merzenich M (1998) Cortical plasticity: From synapses to maps. *Annu Rev Neurosci* 21:149–86.
6. Gilbert CD (1998) Adult cortical dynamics. *Physiol Rev* 78:467–485.
7. Dreher B, Burke W, Calford MB (2001) Cortical plasticity revealed by circumscribed retinal lesions or artificial scotomas. *Prog Brain Res* 134:217–246.
8. Das A, Gilbert CD (1995) Long-range horizontal connections and their role in cortical reorganization revealed by optical recording of cat primary visual cortex. *Nature* 375:780–784.
9. Giannikopoulos DV, Eysel UT (2006) Dynamics and specificity of cortical map reorganization after retinal lesions. *Proc Natl Acad Sci USA* 103:10805–10810.
10. Calford MB, Wright LL, Metha AB, Taglianetti V (2003) Topographic plasticity in primary visual cortex is mediated by local corticocortical connections. *J Neurosci* 23:6434–6442.
11. Calford MB, et al. (2000) Plasticity in adult cat visual cortex (area 17) following circumscribed monocular lesions of all retinal layers. *J Physiol* 524:587–602.
12. Schmid LM, Rosa MGP, Calford MB (1995) Retinal detachment induces massive immediate reorganization in visual cortex. *Neuroreport* 6:1349–1353.
13. Calford MB, Schmid LM, Rosa MGP (1999) Monocular focal retinal lesions induce short-term topographic plasticity in adult cat visual cortex. *Proc Biol Sci* 266:499–507.
14. Keck T, et al. (2008) Massive restructuring of neuronal circuits during functional reorganization of adult visual cortex. *Nat Neurosci* 11:1162–1167.
15. Darian-Smith C, Gilbert CD (1994) Axonal sprouting accompanies functional reorganization in adult cat striate cortex. *Nature* 368:737–740.
16. Grinvald A, Lieke E, Frostig RD, Hildesheim R (1994) Cortical point-spread function and long-range lateral interactions revealed by real-time optical imaging of macaque monkey primary visual cortex. *J Neurosci* 14:2545–2568.
17. Sterkin A, Lampl I, Ferster D, Grinvald A, Arieli (1998) A real time optical imaging in cat visual cortex exhibits high similarity to intracellular activity. *Neurosci Lett* 51:S41.
18. Petersen CCH, Grinvald A, Sakmann B (2003) Spatiotemporal dynamics of sensory responses in layer 2/3 of rat barrel cortex measured in vivo by voltage-sensitive dye imaging combined with whole-cell voltage recordings and neuron reconstructions. *J Neurosci* 23:1298–1309.
19. Jancke D, Chavane F, Naaman S, Grinvald A (2004) Imaging cortical correlates of illusion in early visual cortex. *Nature* 428:423–426.
20. Girman SV, Sauve Y, Lund RD (1999) Receptive field properties of single neurons in rat primary visual cortex. *J Neurophysiol* 82:301–311.
21. Horton JC, Hocking DR (1998) Monocular core zones and binocular border strips in primate striate cortex revealed by the contrasting effects of enucleation, eyelid suture, and retinal laser lesions on cytochrome oxidase activity. *J Neurosci* 18:5433–5455.
22. Smirnakis SM, et al. (2005) Lack of long-term cortical reorganization after macaque retinal lesions. *Nature* 435:300–307.
23. Stepanyants A, Hof PR, Chklovskii DB (2002) Geometry and structural plasticity of synaptic connectivity. *Neuron* 34:275–288.
24. Logothetis NK, Pauls J, Augath M, Trinath T, Oeltermann A (2001) Neurophysiological investigation of the basis of the fMRI signal. *Nature* 412:150–157.
25. Bringuier V, Chavane F, Glaeser L, Fregnac Y (1999) Horizontal propagation of visual activity in the synaptic integration field of area 17 neurons. *Science* 283:695–699.
26. Zur D, Ullman S (2003) Filling-in of retinal scotomas. *Vis Res* 43:971–982.
27. Baker CI, Peli E, Knouf N, Kanwisher NG (2005) Reorganization of visual processing in macular degeneration. *J Neurosci* 25:614–618.
28. Dilks DD, Serences JT, Rosenau BJ, Yantis S, McCloskey M (2007) Human adult cortical reorganization and consequent visual distortion. *J Neurosci* 27:9585–9594.
29. Burkhalter A, Charles V (1990) Organization of local axon collaterals of efferent projection neurons in rat visual cortex. *J Comp Neurol* 302:920–934.
30. Hickmott PW, Steen PA (2005) Large-scale changes in dendritic structure during reorganization of adult somatosensory cortex. *Nat Neurosci* 8:140–142.
31. Tailby C, Wright LL, Metha AB, Calford MB (2005) Activity-dependent maintenance and growth of dendrites in adult cortex. *Proc Natl Acad Sci USA* 102:4631–4636.
32. Hickmott PW, Ethell IM (2006) Dendritic plasticity in the adult neocortex. *Neuroscientist* 12:16–28.
33. Kossut M, Juliano SL (1999) Anatomical correlates of representational map reorganization induced by partial vibrissectomy in the barrel cortex of adult mice. *Neuroscience* 92:807–817.
34. Florence SL, Taub HB, Kaas JH (1998) Large-scale sprouting of cortical connections after peripheral injury in adult macaque monkeys. *Science* 282:1117–1121.
35. Arckens L, et al. (2000) Cooperative changes in GABA, glutamate and activity levels: the missing link in cortical plasticity. *Eur J Neurosci* 12:4222–4232.
36. Massie A, et al. (2003) Glutamate levels and transport in cat (Felis catus) area 17 during cortical reorganization following binocular retinal lesions. *J Neurochem* 84:1387–1397.
37. Massie A, et al. (2003) Extracellular GABA concentrations in area 17 of cat visual cortex during topographic map reorganization following binocular central retinal lesioning. *Brain Res* 976:100–108.
38. Rosier AM, et al. (1995) Effect of sensory deafferentation on immunoreactivity of GABAergic cells and on GABA receptors in the adult cat visual cortex. *J Comp Neurol* 359:476–489.
39. Benali A, Weiler E, Benali Y, Dinse HR, Eysel UT (2008) Excitation and inhibition jointly regulate cortical reorganization in adult rats. *J Neurosci* 28:12284–12293.
40. Hirsch JA, Gilbert CD (1993) Long-term changes in synaptic strength along specific intrinsic pathways in the cat visual cortex. *J Physiol (London)* 461:247–262.
41. Celikel T, Szostak VA, Feldman DE (2004) Modulation of spike timing by sensory deprivation during induction of cortical map plasticity. *Nat Neurosci* 7:534–541.
42. Young JM, et al. (2007) Cortical reorganization consistent with spike timing–but not correlation-dependent plasticity. *Nat Neurosci* 10:887–895.